Transition Spectra in the Vibrational Quasicontinuum of Polyatomic Molecules. IR Multiple-Photon Absorption in SF_6. 2. Theoretical Simulation and Comparison with Experiment

V. N. Lokhman, A. A. Makarov, I. Yu. Petrova, E. A. Ryabov, and V. S. Letokhov*

Institute of Spectroscopy, Russian Academy of Sciences, 142092 Troitsk, Moscow Region, Russia

Received: June 30, 1999; In Final Form: September 29, 1999

The IR MP excitation spectra of the SF_6 molecule in the vibrational quasicontinuum (QC) measured experimentally in the vicinity of the ν_3 mode frequency are compared with their theoretical counterparts with a view to revealing the relative contribution from the statistical inhomogeneous broadening (SIB) and homogeneous broadening to the formation of the IR transition spectra in the QC. The IR MP spectra are found by solving rate equations, the cross sections of the successive transitions being calculated in the SIB approximation. The half-width γ_L of the Lorentzian profile associated with the homogeneous broadening is the only adjustment parameter of the model. A good agreement (within the accuracy of measurement) is obtained between the experimental and theoretical IR MP spectra over a wide range of spectral and energy parameters. The γ_L values are found which vary within the limits $0.53 \leq \gamma_L \leq 10.2$ cm^{-1} in the energy range $4500 \leq E \leq 30\,000$ cm^{-1}. The conclusion is drawn that the main parameters of the IR transition spectra in the QC (the position of the maximum, width, and intensity) are governed largely by the SIB effect, though the Lorentzian wings may play a decisive role when excitation occurs at the edges of the spectrum. The IR transition cross sections found are used to compute the IR MP excitation dynamics in the QC and determine the vibrational distribution function being formed. It is found that excitation in the QC may also give rise to a nonequilibrium bimodal distribution.

1. Introduction

This work is a continuation of our publications[1,2] devoted to the studies of the spectral characteristics of vibrational transitions in the quasicontinuum (QC → QC transitions) of polyatomic molecules. The objects of our studies were molecules the type of XY_6, specifically the SF_6 molecule. An approach was developed in ref 1 that made it possible to calculate the main parameters—the intensity, shape, and position of QC → QC transition profiles—in the approximation where the predominant part is played by the statistical inhomogeneous broadening (SIB). Recall that this type of broadening is associated with the dispersion of the frequencies of transitions from a given chaotic vibrational state that is contributed to by a large number of harmonic states with various sets of occupation numbers in the modes (for details, see ref 1 and references therein). The correctness of the approach developed was verified by comparing between experimental and theoretical Raman spectra in the neighborhood of the frequency of the ν_1 mode of highly excited SF_6 molecules.[2] The same investigations allowed us to conclude that in SF_6 the principal contribution to the shape of transition spectra in the QC was made exactly by the SIB effect, the contribution from the homogeneous broadening associated with the IVR process being substantially smaller.

The present work is devoted to the study of the spectra of IR active transitions in the QC of the SF_6 molecule in the vicinity of the frequency of the ν_3 mode. The main objective of the work is to reveal the contribution from the homogeneous broadening to the shape of QC → QC transition spectra. To this end, we study the IR multiple-photon (MP) absorption in SF_6 molecules preliminarily excited into the QC (see Figure 1 in ref 3). The idea of using such an approach is based on the possibility of accumulation of the relatively small contribution to the transition profiles from the Lorentzian wings associated with the homogeneous broadening as a result of a large number of transitions up the ladder of vibrational states in the course of IR MP excitation in the QC. Information on the homogeneous broadening parameters was expected to be obtained from comparison between experimental and theoretical IR MP absorption spectra. The results obtained within the framework of the approach described are presented in two papers. The first (the preceding paper[3]) presents the results of measuring IR MP absorption in the quasicontinuum of SF_6 over a wide range of both the level of preliminary excitation into the QC and the fluence and frequency of the exciting laser radiation. The second part of the work (the present paper) presents the results of comparison between the experimental data on IR MP excitation in the QC of SF_6 and theoretical calculations based on the IR MP excitation model developed.

The approach used in this work to describe the IR MP excitation dynamics is based on the use of rate equations. Rate equations were used for the first time to describe the IR MP excitation and dissociation processes in ref 4 when interpreting the experiment with SF_6. The derivation of these equations (on first principles), as well as the substantiation of the possibility of using them for various types of molecules and various excitation conditions can be found in refs 5 and 6 (see also ref 7). Later on, rate equations have been used frequently enough to describe and interpret experiments on the IR MP excitation and dissociation of molecules. A review of the appropriate works can be found, for example, in refs 7−9. Use is usually made of

* FAX: +(095)334-0886. E-mail: letokhov@isan.troitsk.ru.

10.1021/jp9922460 CCC: $18.00
Published on Web 12/03/1999

the approximation where IR MP excitation is considered as an incoherent process of consecutive single-quantum transitions up the ladder of some "levels". The distance between these "levels" is equal to the quantum energy of the exciting radiation, and their "degeneracy" is taken to be proportional to the density of vibrational or rovibrational states near these "levels". It is also assumed that the rates of both direct and inverse processes are linearly related to the radiation intensity, and the ratio of these rates obeys the detailed balancing principle. Though this approximation holds, strictly speaking, for the description of excitation in the QC above its boundary E_{QC} (case B in the notations of ref 6), it is being frequently used to describe the dynamics of the IR MP excitation of molecules, starting with their ground state.

The main problem in using rate equations is associated with the choice of the cross sections of the successive transitions. Starting with the work reported in ref 4, many papers used an empirical approach where the transition cross sections (the law governing their variation with energy) were selected by some method, sometimes arbitrary enough, in no way related to the spectroscopic parameters of the molecule in hand. The unknown parameters entering into the transition cross sections were then found by fitting experiment and theory. This approach has a number of essential shortcomings associated first of all with the arbitrariness in choosing the cross sections. Specifically, the fitting parameters obtained for some laser radiation frequency may prove inadequate to the description of the IR MP excitation process at other frequencies. Subsequently, another, more realistic approach was suggested to the selection of transition cross section (see, e.g., refs 10−12), which may be referred to as a semiempirical approach. In particular, when interpreting experiments with CF_3I in ref 10, the cross section values were calculated on the basis of the actual spectroscopic parameters of the molecule. Note that the authors of ref 10 also suggested an approach that allowed the problem of modeling the MP excitation in the region below the QC boundary in comparing theory and experiment to be circumvented. As for the shape of the transition band profile, it was assumed to be Lorentzian: it was exactly the parameters of this profile that were taken to serve as the fitting parameters in comparing theory and experiment. The Lorentzian shape of the transition band profile was also used in ref 11 when interpreting experiments with SF_6. So, it also proved impossible in this semiempirical approach to avoid some arbitrariness associated with the selection of the transition profile shape. It should be noted that the uncertainty in selecting the spectral shape of the cross sections of successive transitions, associated with the impossibility of the a priori computation of this shape for a particular molecule, still remains to the present day.

The approach used in this work to the rate-equation description of the IR MP excitation dynamics in the quasicontinuum of the SF_6 molecules is distinguished by the fact that the cross sections of all the consecutive transitions are wholly calculated (in the SIB approximation) on the basis of the actual spectroscopic characteristics of this molecule, as described in ref 1. The contribution from the homogeneous broadening to the transition cross sections is in that case treated as a correction, and the magnitude of this contribution is essentially the only adjustment parameter of the model. We believe that the allowance for the homogeneous broadening in the form of a correction to the SIB is quite justified. That this conclusion holds true for the Raman active mode ν_1 is supported by the data presented in ref 2. As regards the IR active mode ν_3 of interest to us, we may cite the width estimates made in ref 13 for the Lorentzian profile associated with the homogeneous broadening. For example, at a molecular vibrational energy of $E = 10\,000$ cm^{-1} this estimate of the width of the Lorentzian profile is $2\gamma_d = 2$ cm^{-1}, while the width of the Gaussian profile associated with the SIB at the same molecular energy is $2\sigma_0 = 12.8$ cm^{-1}.[1] It should be noted at the same time that according to this estimate the homogeneous broadening and the associated IVR rate are sufficiently great for the excitation incoherence condition $2\gamma_d \gg W$ to be satisfied, W being the characteristic radiative excitation rate. Simple estimates show that this condition is fulfilled by a wide margin, no matter what the experimental conditions.[3]

This paper is designed as follows. Section 2 describes the IR MP excitation model used. The need to allow for the rotational structure of transitions materially increased the number of equations to be solved. Their solution algorithm providing for computation on modern personal computers is presented in Appendix B. Section 3 describes the procedure of fitting model computations and experimental data[3] and presents the results obtained. The paper ends with the discussion of the results (section 4) and conclusions (section 5).

2. Model of IR MP Excitation of Molecules in the Quasicontinuum

As noted earlier, to describe the IR MP excitation dynamics, use is made in the present work of rate equations. These equations describe the change of the populations of groups of levels whose vibrational energies differ by an amount equal to the laser radiation quantum $\hbar\omega$ (see Figure 1). These groups are identified by two subscripts: n and J. The first subscript n denotes the number of quanta needed to be absorbed in order to get from the initial state to the state of the n group. By the initial state is usually meant the QC boundary, i.e., E_{QC}, but formally this can be the ground state as well (see later in the text). The second subscript J denotes the rotational quantum number, which varies by the selection rules $J \rightarrow J, J \pm 1$. The groups of levels in Figure 1 are coupled together by stimulated transitions whose rate is $W = \sigma P$, where σ is the transition cross section and P is the photon flux density of laser radiation. The cross section of transitions at a frequency of ν (in cm^{-1}) from vibrational states with an energy of E may be written as

$$\sigma(\nu,E) = \frac{4\pi^2\nu}{\hbar c}\mu_0^2 G(\nu,E) \qquad (1)$$

where μ_0 is the dipole moment of the transition $0 \rightarrow 1$, and $G(\nu,E)$ is the spectral intensity of the transition band. We have earlier suggested in ref 1 a procedure for computing the intensity of QC → QC transitions in the SIB approximation. Computations for the transition band of the mode ν_3 in SF_6 have shown that the spectral intensity of this band can be well described by the Gaussian function

$$G(\nu,E) = \frac{I_0(E)}{\sqrt{2\pi}\sigma_0(E)} \exp\left[-\frac{(\nu - \nu_m(E))^2}{2\sigma_0^2(E)}\right] \qquad (2)$$

where I_0 is the integral intensity of the band, $\nu_m(E)$ is the position of the maximum, and $2\sigma_0(E)$ is the width of the band (in cm^{-1}), I_0, ν_m, and σ_0 being functions of the vibrational energy E of the molecule. The values of these parameters (upward transitions) have been computed in ref 1 for purely vibrational transitions of the ν_3 band without regard for rotations. Formally, this means that the rotational constant B_0 and the Coriolis constant ξ_3 are equal to zero. In the case where B_0 and ξ_3 are nonzero, there

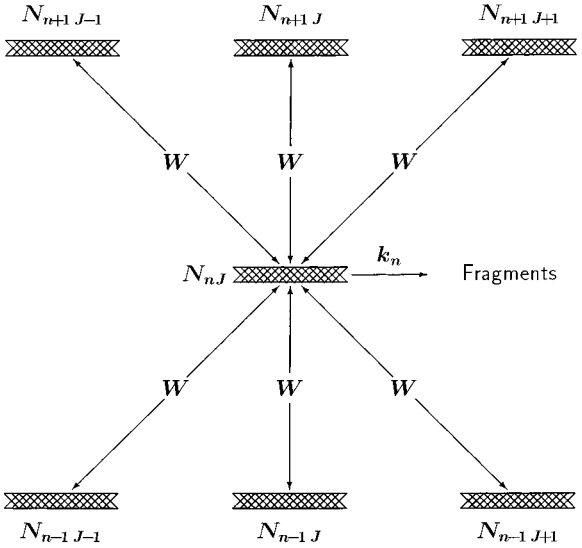

Figure 1. Schematic diagram of transitions in the vibrational quasicontinuum.

takes place the redistribution of the integral intensity I_0 over the three rotational branches P, Q, and R. We can demonstrate that the intensity of transitions from a state with a given J in these three branches are related as

$$I_P:I_Q:I_R = \frac{2J-1}{3(2J+1)}:\frac{1}{3}:\frac{2J+3}{3(2J+1)} \tag{3}$$

For each of these three transitions, there occurs an additional frequency shift relative to ν_m. It consists of the term $\Delta\nu_{cor} \simeq -B_0\xi_3(\bar{n}_3+2)$ ($\bar{n}_3$ being the average occupation number in the mode ν_3 for a given E), the same for all the three branches. Besides, for the P and R branches, there are the additional terms

$$\Delta\nu_P \simeq -2(1-\xi_3)B_0J \qquad \Delta\nu_R = 2(1-\xi_3)B_0(J+1) \tag{4}$$

responsible for the usual PQR structure of the vibrational band. Considering the additions made, the procedure suggested in ref 1 enables one to calculate stimulated transition rates for quasicontinuum states with specified E and J and for specified laser radiation intensity and frequency in the vicinity of the ν_3 mode. Note that for any laser radiation frequency $\omega \approx \omega_3$, the rates of upward and downward transitions between any pair of groups of levels (Figure 1) with an energy of E and $E+\hbar\omega_3$ are related as

$$\frac{W(nJ \rightarrow n'J')}{W(nJ \leftarrow n'J')} = \frac{\rho(n')}{\rho(n)}\frac{2J'+1}{2J+1} \tag{5}$$

The "rotational" term for the P and the R branch in (5) results from the difference in degeneracy between levels with different J's. The same effect is responsible for the unequal redistribution of the integral transition intensity between these branches in (3). The "vibrational" term

$$\frac{W_{up}(E)}{W_{down}(E+\hbar\omega_3)} = \frac{\rho(E+\hbar\omega_3)}{\rho(E)} \tag{6}$$

follows from the detailed balancing principle. It can be shown that for the triply degenerate mode ν_3,

$$\frac{\rho(E+\hbar\omega_3)}{\rho(E)} = \frac{\bar{n}_3(E)+3}{\bar{n}_3(E+\hbar\omega_3)} \tag{7}$$

Finally, using the notation of Figure 1, we may write down the following equations for the populations N_{nJ}:

$$\frac{dN_{nJ}}{dt} = \sum_{J'=J-1}^{J+1} W_{n-1,J'}^{nJ}N_{n-1,J'} - \left(\sum_{J'=J-1}^{J+1} W_{nJ}^{n-1,J'}\right)N_{nJ} + \sum_{J'=J-1}^{J+1} W_{n+1,J'}^{nJ}N_{n+1,J'} - \left(\sum_{J'=J-1}^{J+1} W_{nJ}^{n+1,J'}\right)N_{nJ} - k_nN_{nJ} \tag{8}$$

where the term k_nN_{nJ} describes the unimolecular decay of molecules from the nth group, provided that their energy exceeds the dissociation energy D_0; otherwise, $k_n \equiv 0$. The total dissociation yield from the nth group is found by summing with respect to J:

$$\frac{dY_n}{dt} = k_n\sum_J N_{nJ} \tag{9}$$

The maximum $n = n_{max}$ in (8) was selected such that

$$k_{n_{max}} \gg \sum_{J'} W(n_{max},J \rightarrow n_{max}+1,J') \tag{10}$$

Indeed, the population distribution in that case actually never reaches the group with $n = n_{max}$. The values of the unimolecular decay rate constant k_n were calculated by the RRKM theory (see Appendix A). The maximum k_n value in (10) was taken to be $k_{n_{max}} \simeq 10^{10}$ s^{-1}, which was substantially higher than the values of the stimulated transition rate W actually reached in our experiments. Using the functions $k_n = k(E)$ calculated, one can easily find that $n_{max} \approx 60$.

Let us now estimate the number of equations (8) to be solved. Insofar as the experiment was conducted at an initial temperature equal to room value, it is necessary to give consideration in the model for the initial distribution of the molecules among the rotational levels J. It is but natural to terminate this distribution at some $J = J_{max}^{(0)}$ such that the overwhelming majority of the molecules are at $J \le J_{max}^{(0)}$. To illustrate, in the case of a Boltzmann distribution with $T_{rot} = 300$ K, account is taken of 99% of the molecules if $J_{max}^{(0)} \simeq 120$. Subsequently, the excitation process starts involving states with even higher J values, up to $J_{max} \simeq J_{max}^{(0)} + n_{max}$, because transitions in the R branch can take place upon absorption of each new quantum. As a result, the need arises to simultaneously solve about 10 000 equations (8). So great an amount of equations to be solved simultaneously required the use of a special algorithm, which is described in Appendix B.

3. Model Calculations and Their Comparison with Experimental Data

Before proceeding to the description of the procedure of comparing between experimental data and model calculations, let us recall how the experiment was conducted (for details, see ref 3). With a pump pulse at a frequency of ω_1 (the 10P-(16) CO_2 laser line), the SF_6 molecules were excited into the quasicontinuum (see Figure 1 in ref 3). After the lapse of some time τ_d long enough for an equilibrium *vibrational* distribution to be established, a probe pulse of frequency ω_2 was passed through the excited region. We measured the average number N_2 of quanta (per molecule) absorbed in the probe volume as a function of the level of preliminary excitation into the QC n_1-(ϕ_1) (n_1 is the average number of quanta absorbed from the pump pulse and ϕ_1 is the *local* value of the fluence of the latter), the fluence Φ_2 of the probe pulse, and its frequency ω_2. The

TABLE 1: Frequencies and Anharmonicity Constants of SF_6 Used To Calculate Vibrational Transition Profiles

	mode (i)					
	1	2	3	4	5	6
ν_i (cm^{-1})	774.54[a]	643.35[a]	948.10[b]	615.02[a]	523.56[a]	346.08[a]
x_{3i} (cm^{-1})	−2.902[c]	−3.603[c]	−1.7468[b]	−1.52[c]	−1.2[c]	−1.102[c]

[a] Borrowed from ref 14. [b] Borrowed from ref 15. [c] Borrowed from ref 16.

experiment was performed with Gaussian beams, and so the volume of the probe region in determining the parameter $N_2(n_1,\Phi_2,\omega_2)$ was taken to be $V_2 = S_2L$, where L is the length of the absorption cell and S_2 is the cross-sectional area of the Gaussian beam ($S_2 = 2\pi a_{02}^2$, and a_{02} is the beam radius at a level of $1/e$). The fluence Φ_2 was defined as $\Phi_2 = E_2/S_2$, where E_2 is the energy of the probe pulse. Thus, the parameter $N_2(n_1,\Phi_2,\omega_2)$ being determined in the experiment is in fact the result of averaging over the spatially inhomogeneous distribution of both the probe and the pump beam, through the intermediary of the quantity $n_1(\phi_1)$ in the latter case.

Comparison between theory and experiment was carried out by comparing the measured N_2 values with their computed counterparts. Using the adjustment parameters of the model, the best fit was found between N_2^{exp} and N_2^{th} over the entire range of the n_1, Φ_2, and ω_2 values. Note that the IR MP excitation model described above makes it possible to compute only the *local* values of the number of quanta, $n_2 = n_2(\phi_2,n_1,\omega_2)$, absorbed from the probe pulse for the given *local* values of its fluence $\phi_2 = \phi_2(x,y,z)$ and n_1 as well. Therefore, the values of $n_2 = n_2(\phi_2,n_1,\omega_2)$ found were used as a database for computing N_2 with due regard for the spatial distribution of both the pump and the probe beam.

3.1. Computation of Local Parameters. The local values of the average number $n_2 = n_2(\phi_2,n_1,\omega_2)$ of absorbed quanta were calculated by solving equations (8). We first computed the cross sections of upward and downward transitions in the vicinity of the triply degenerate mode ν_3. The spectral intensity of the vibrational transition band, $G(\nu,E)$, in (1) was calculated in the SIB approximation. In the region of vibrational energies $E \geq 7000$ cm^{-1}, calculation was carried out in accordance with the procedure described in ref 1. Note that because of the high density of vibrational states, not all of them were taken into consideration in calculations, but only their random sample. At $E < 7000$ cm^{-1}, all the states were taken into account. As a result of these calculations, it was found that the shape of the transition band could be well described by Gaussian function (2) as E was decreased down to $E = 4000$ cm^{-1}, the profile parameters I_0, σ_0, and ν_m being well approximated by linear functions the type of $(a + bE)$. Rate equations (8) hold true in describing the dynamics of IR MP excitation above the QC boundary, but for the sake of convenience we used them starting with the ground state. The error due to this approximation is small, for, as will be demonstrated in the text to follow, comparison between theory and experiment was in most cases carried out in conditions where the contribution from the molecules with an initial energy of $E < E_{QC}$ was insignificant. The vibrational frequencies and intermode anharmonicity constants used in calculating the parameters of the function $G(\nu,E)$ are listed in Table 1. As to the anharmonic constants G_{33} and T_{33} responsible for the splitting of the mode ν_3, their values were taken to be $G_{33} = 0.9262$ cm^{-1} and $T_{33} = -0.2487$ cm^{-1}.[15] The values of the parameters of the function $G(\nu,E)$ finally used in solving equations (8) are presented in Table 2. When the absolute values of transition cross section (1) were calculated, the transition dipole moment μ_{01} was taken at 0.388 D.[17] To allow for the possible contribution from the homogeneous broadening, Gaussian profile (2) was convolved with the Lorentzian profile

$$L(\nu,E) = \frac{\gamma_L(E)}{\pi} \frac{1}{\gamma_L^2(E) + (\nu - \nu'_m)^2} \qquad (11)$$

It should be noted that this approach is approved, at least, in our case when expected IVR rates are much smaller than the width due to SIB. The argument is that a relevant theoretical model[18] (anharmonic oscillator linearly relaxing in the thermal bath) always gives, at wings of the absorption spectrum, the single-Lorentzian asymptotics. So, convolution of the SIB contour with a relatively narrow Lorentzian is a quite natural parametrization for our problem as long as this procedure does not significantly change the peak and provides the expected asymptotics at the wings.

The molecular energy-dependent profile half-width $\gamma_L(E)$ in (11) is the fitting parameter of the model. The procedure used to allow for the rotational structure of the transitions in (8) has been described above. The values of the rotational and Coriolis constants used in calculations were borrowed from ref 19 to be $B_0 = 0.091\,084$ cm^{-1} and $\xi_3 = 0.693\,44$ cm^{-1}.

When equations (8) were solved, the molecular energy was specified by an integral number of quanta at the probe laser radiation frequency ω_2. Accordingly, the initial Boltzmann distribution was also assumed to be discrete, and the population of these "levels" was computed using the vibrational temperature T_{vib} reached by the instant the probe pulse arrived. The value of this vibrational temperature T_{vib}, as well as that of the rotational temperature T_{rot}, was determined from the energy balance with due regard for the energy absorbed from the probe pulse and that stored in the vibrational, rotational, and translational degrees of freedom at room temperature. The "heating" of the translational and rotational degrees of freedom as a result of the V−T/R relaxation was calculated on the basis of the rate constant of this process in SF_6 measured in ref 20. Because the rate of this process is slow, its consideration in our experimental conditions ($p = 1$ Torr, $\tau_d = 5$ μs) only led to an insignificant (2−3%) decrease of T_{vib}. The increase of the rotational temperature, ΔT_{rot}, was more substantial and amounted, for example, to some 100 K at $n_1 = 9$ quanta.

When equations (8) were solved, the temporal shape of the probe pulse was taken to be Gaussian and have a duration of $\tau = 200$ ns (fwhm); the dissociation energy was taken to be $D_0 = 91.3$ kcal/mol.[21]

3.2. Allowance for Spatial Nonuniformity and the Fitting Procedure. As already noted, solving equations (8) enables one to find local values of the absorption $n_2 = n_2(\phi_2,n_1,\omega_2)$ at various values of the parameters ϕ_2, n_1, and ω_2. At the same time, it also makes it possible to determine the dissociation yield, both the total and that during the pulse. The number N_2^{th} of quanta absorbed in the volume being probed was calculated as follows. First, on the basis of the function $n_1 = n_1(\phi_1)$ measured (curve 2 of Figure 4 in ref 3), we calculated the transverse distribution of T_{vib} and T_{rot} for a Gaussian pump beam profile at a number of specified values of n_1 on the *beam axis*. Thereafter, using the database available on the local values of $n_2(\phi_2,n_1,\omega_2)$, we calculated the energy ΔE_2 absorbed from the probe pulse at specified values of its fluence Φ_2, account being taken of the reduction of probe pulse intensity along the length of the absorption cell. (Recall that Φ_2 is defined as $\Phi_2 = E_2/2\pi a_{02}^2$, where E_2 is the pulse energy and a_{02} is the beam radius at a

TABLE 2: Numerical Parameters[a] for Gaussian Transition Profiles

		maximum frequency, ν_m[b]		half-width, σ_0[b]		intensity, I_0[c]	
transition		a	$b\times10^3$	a	$b\times10^3$	a	$b\times10^3$
upward	$E^b \geq 7000$	948.3625	−3.13	1.705	0.47	0.86	0.07
	$E^b < 7000$	948.005	−3.08	0.65	0.62	0.93	0.063
downward	$E^b \geq 7000$	951.2125	−3.11	1.195	0.475	−0.1	0.065
	$E^b < 7000$	951.4785	−3.17	0.137	0.616	−0.079	0.064

[a] The maximum frequency ν_m, half-width σ_0, and integral intensity I_0 of Gaussian transition profile (2) are linearly interpolated by the formula $(a + bE)$ with the vibrational energy E in cm^{-1}. [b] In cm^{-1}. [c] In units of μ_{01}^2, the squared transition dipole moment of the ν_3 mode.

level of $1/e$.) The value of ΔE_2^{th} thus obtained was used to find the sought-for value of $N_2^{th} = \Delta E_2^{th}/(2\pi a_{02}^2 NL)$, where N is the density of the molecules and L is the length of the absorption cell. It should be emphasized that when the quantity ΔE_2 was calculated, account was taken of the actual probe beam profile, including its difference from the Gaussian profile in the wings (see expression (2) in ref 3).

For comparison and subsequent adjustment of the experimentally measured and computed data, use was made of the relationship $N_2 = N_2(n_1)$ for a number of fixed values of Φ_2 (see Figure 2): 0.1, 0.25, and 0.5 J/cm^2. At $\Phi_2 = 0.1$ J/cm^2 absorption already takes place in a multiple-photon fashion, and at $\Phi_2 = 0.5$ J/cm^2 the dissociation yield *during the pulse* is still too low to distort the measurement process, e.g., on account of absorption by the SF_5 radicals formed. The parameter $\Delta = |N_2^{exp} - N_2^{th}|/N_2^{exp}$ was taken to serve as a measure of discrepancy between the experimental and theoretical N_2 values. Next, we found the quantity Δ for each of the three Φ_2 values for integer n_1 values in the range $l \leq n_1 \leq m$ and determined the mean deviation $\langle\Delta\rangle$:

$$\langle\Delta\rangle = \frac{1}{3}\sum_{i=1}^{3}\frac{1}{m-l+1}\sum_{n_1=l}^{m}\Delta(n_1,\Phi_2^{(i)}) \qquad (12)$$

To provide for correctness of comparison between the model and experiment, the value of l in most cases was taken equal to 6. Under such conditions, more than 70% of the molecules have an energy of $E \geq 5000$ cm^{-1}. The value of m was taken to be equal to 12 to limit the possible contribution from the dissociation of the molecules.

The fitting procedure was aimed at attaining minimal $\langle\Delta\rangle$ values for all the frequencies ω_2, the set of fitting parameters naturally being the same for all the frequencies. As follows from what has been said above, the only unknown model parameter that can be used to serve for fitting purposes is the contribution from the homogeneous broadening, i.e., the half-width $\gamma_L(E)$ of the corresponding Lorentzian contour. The rest of the model parameters were either measured directly or calculated on the basis of experimentally measured quantities. In principle, these quantities were measured with some error, which may give some additional degrees of freedom in fitting. Most sensitive in this sense may be the Gaussian profile parameters, namely, the width $2\sigma_0$ of the profile and the position of its maximum, ν_m. However the values of the anharmonic constants x_{ij}, which determine the magnitudes of $2\sigma_0$ and ν_m, are given in the literature with a high degree of accuracy. Our calculations have shown that the variation of the x_{ij} values within the limits of the error indicated have practically no effect on the N_2^{th} values calculated. We may also point out another two possibilities, namely, the inaccuracy in determining the transition dipole moment μ_{01} and the error of energy measurements. As reported in ref 17, the error in measuring μ_{01} amounts to ±5%. The accuracy of the absolute calibration of the calorimeter used is somewhat worse: according to the manufacturer, it lies within 20%. However, varying any of these two parameters gives rise to a systematic shift of the theoretical or experimental curves of Figure 2, this shift having the same sign for all the frequencies ω_2. At the same time, the remaining discrepancy between the N_2^{exp} and N_2^{th} curves differs in sign between different ω_2 (see later in the text) and is most likely not associated with the effect of the last two factors. For this reason, they were left as they were, and the experimental and theoretical data were finally fitted by varying the only factor—the magnitude of the homogeneous broadening.

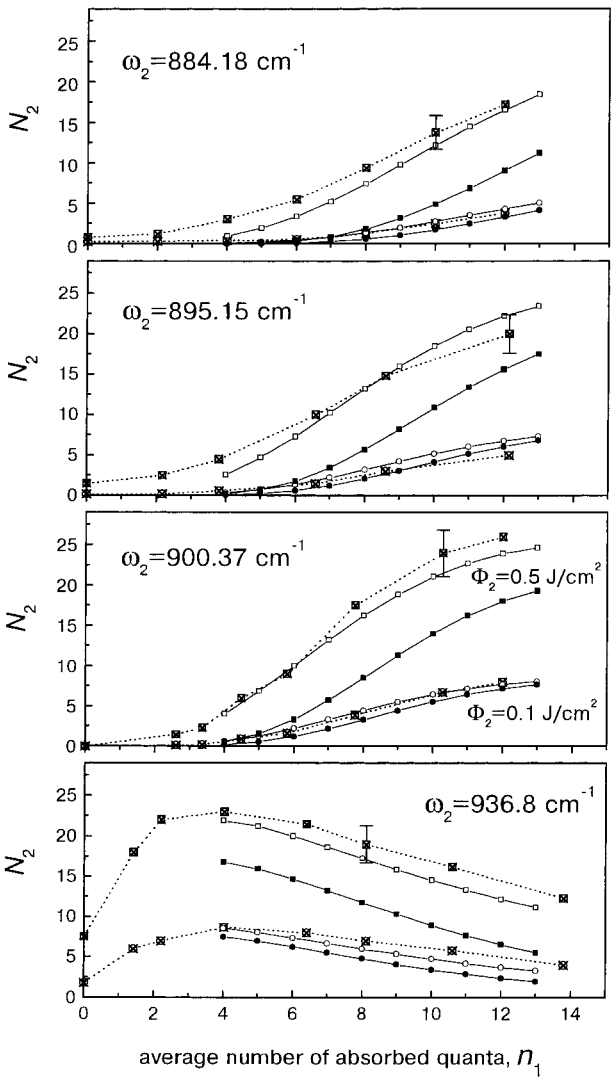

Figure 2. Number N_2 of quanta absorbed from the probe pulse as a function of the preliminary excitation level n_1 for various values of the frequency ω_2 and fluence Φ_2. Dashed curves and crossed symbols: experiment. Solid curves: calculation. Filled symbols: allowance made for the SIB effect only. Open symbols: allowance made for both the SIB and homogeneous broadening effects with γ_L defined by eq 13. Squares: $\Phi_2 = 0.5$ J/cm^2. Circles: $\Phi_2 = 0.1$ J/cm^2.

3.3. Results of Fitting. Figure 2 presents experimental relationships (dashed curves, crossed symbols) between the average number N_2^{exp} of quanta absorbed from the probe pulse and the preexcitation level n_1 for two values of the probe pulse fluence Φ_2: 0.1 and 0.5 J/cm^2. (Recall that n_1 is the average number of quanta absorbed from the pump pulse on the beam axis.) These relationships are presented for several values of the frequency ω_2 corresponding to the "blue" ($\omega_2 = 936.8$ cm^{-1}) and "red" wings of the MP absorption spectrum (see Figure 5 below). As can be seen, the character of the function $N_2^{exp} = N_2^{exp}(n_1)$ differs even qualitatively between different parts of the MP spectrum. At the "blue" end N_2^{exp} first rises to reach its maximum and then, starting with $n_1 \approx 4$, the absorbed energy begins to drop with increasing n_1. Reducing the frequency ω_2 causes the maximum of the function $N_2^{exp} = N_2^{exp}(n_1)$ to shift toward higher n_1 values, and as one goes further into the long-wavelength region, this maximum is not reached altogether (see also Figure 6 in ref 3). Figure 2 also presents the theoretical values N_2^{th} calculated for two cases, namely, in the statistical inhomogeneous broadening approximation, i.e., at $\gamma_L = 0$ (filled symbols), and with due regard for the homogeneous broadening (open symbols). It can be seen that the allowance for the SIB effect alone qualitatively correctly conveys the character of the function $N_2 = N_2(n_1)$. At the same time, a perceptible quantitative discrepancy is observed between N_2^{exp} and N_2^{th}, which increases as Φ_2 is increased and as one goes further into the "red" region of the spectrum. The latter circumstance obviously points to the fact that consideration of the inhomogeneous broadening only cannot help correctly describe the IR MP excitation process in the wings of the absorption band.

The homogeneous broadening was taken into consideration as follows. It was assumed in the model that those molecules that had absorbed more than four quanta moved into their quasicontinuum, which agreed with $E_{QC} = 5000 \pm 500$ cm^{-1}.[22] Therefore, the homogeneous broadening was formally "switched on" in a stepwise fashion starting with $E = 4400$ cm^{-1}. The sought-for parameter $\gamma_L(E)$—the Lorentzian profile half-width—was varied in the course of the fitting procedure over the range of values confined between the dash-and-dot lines in Figure 3. The upper boundary of this region approximately corresponds to the inhomogeneous half-width σ_0 and the lower, to the estimates of a "dissipative" γ_d obtained in ref 13.

Next the γ_L values were varied within the limits of the above region (as a rule, use was made of various linear $\gamma_L - E$ relations the type $(a + bE)$) with a view to minimizing the value of the criterion $\langle\Delta\rangle$ (12) for all the frequencies ω_2 used. Within the range of the parameters n_1 and Φ_2 selected by us, the fitting results proved most sensitive to the variation of γ_L over the molecular energy range 4500 cm^{-1} < E < 15 000 cm^{-1}. This made it possible to provide for a higher reliability in determining γ_L in this energy region and conclude in particular that the dependence of γ_L on E was in this range faster than linear. As a final analysis, the solid curve in Figure 3 shows the function $\gamma_L = \gamma_L(E)$ found to provide for the best fit between the theoretical and experimental N_2 values. This function may be represented in the form

$$\gamma_L(E) = \begin{cases} 0.9 - 2.3 \times 10^{-4}E + 3.3 \times 10^{-8}E^2 & 4500 \le E \le 10000 \text{ cm}^{-1} \\ -2.23 + 4.14 \times 10^{-4}E & 10000 < E \end{cases} \quad (13)$$

The quantity γ_L changes from 0.53 to 10.2 cm^{-1} as E is varied from 4500 to 30 000 cm^{-1}. (The uncertainty estimated by us in determining γ_L is shown in Figure 3 by the vertical straight lines.) Note that the inhomogeneous broadening σ_0 varies from 3.44 to 15.7 cm^{-1} over the same range of E values.

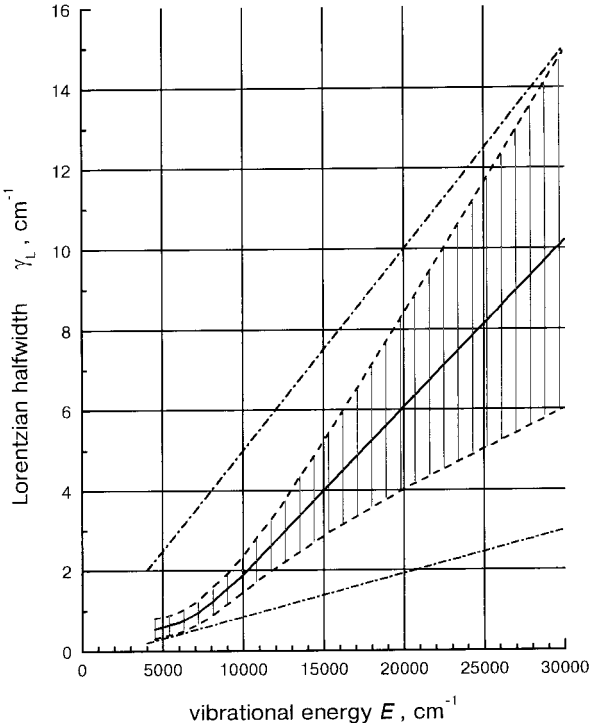

Figure 3. Lorentzian profile half-width γ_L (solid curve) as a function of the vibrational energy E. Dash-and-dot lines: limits of variation of γ_L in fitting the experiment and model. Dashed curves: estimates of the inaccuracy of determining γ_L.

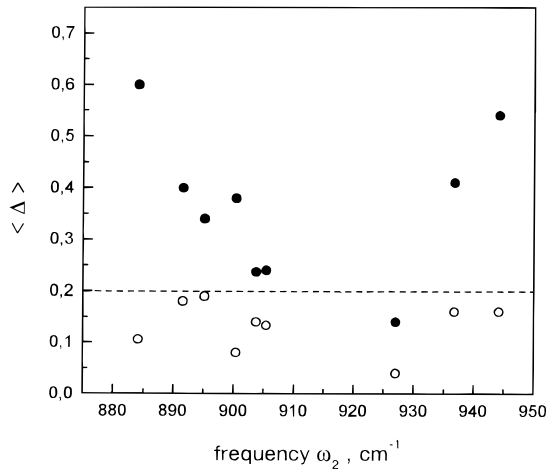

Figure 4. Parameter $\langle\Delta\rangle$ (see (12)) of the mean deviation of calculated N_2 values from their experimental counterparts as a function of the radiation frequency ω_2. Filled circles: calculation with allowance made for the SIB effect only. Open circles: calculation with allowance made for both the SIB and homogeneous broadening effects.

The N_2^{th} values calculated with due regard for the homogeneous broadening and indicated in Figure 2 by open symbols were obtained precisely for the best-fit values of γ_L (13). Obviously, consideration of the homogeneous broadening in that case provides for *quantitative* agreement with experiment over a wide range of the parameters ω_2, Φ_2, and n_1. This conclusion is supported by Figure 4, which presents the values of $\langle\Delta\rangle$ for all the frequencies ω_2 used with and without regard for the homogeneous broadening. It can be seen that the magnitude of $\langle\Delta\rangle$ in taking account of the homogeneous broadening with γ_L according with (13) nowhere exceeds 20% and on the average

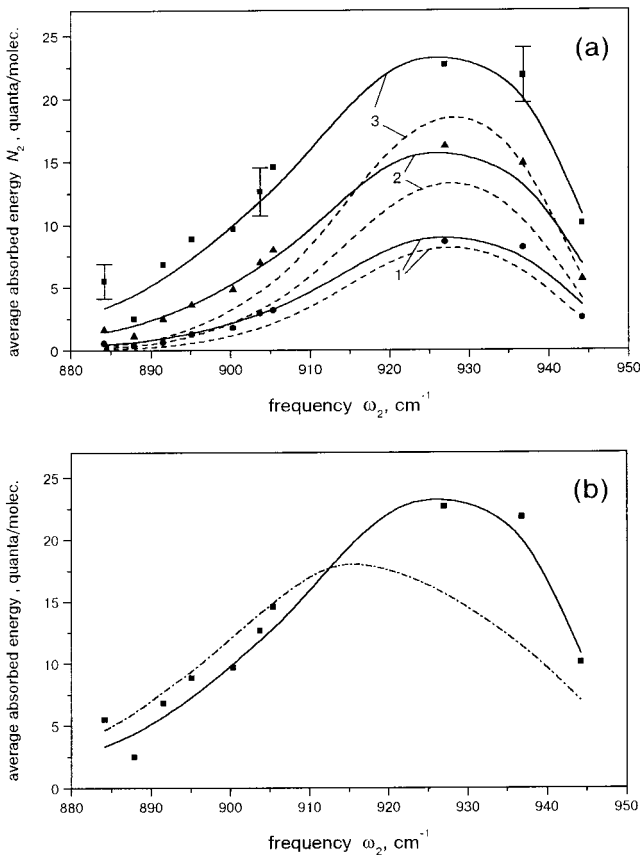

Figure 5. IR MP absorption spectra for SF_6 at a preexcitation level of $n_1 = 6$ quanta ($T_{vib} = 960$ K). (a) Symbols: experimental N_2 values. Dashed curves: calculation with allowance made for the SIB effect only. Solid curves: calculation with allowance made for both the SIB and homogeneous broadening effects with γ_L defined by eq 13. Fluence Φ_2: (1) 0.1 J/cm^2; (2) 0.25 J/cm^2; (3) 0.5 J/cm^2. (b) Demonstrating the role of the nonuniform spatial distribution of radiation. Symbols and solid curve: experiment and calculation for actual beams (see text) at $\Phi_2 = 0.5$ J/cm^2. Dash-and-dot curve: calculation for uniform distributions of the pump and probe beams at $\phi_2 = 0.5$ J/cm^2.

(over all the ω_2 values used) amounts to 13%. Consideration of only the SIB effect ($\gamma_L = 0$) may give rise to a substantial discrepancy between the theoretical and experimental N_2 values, especially at the ends of the IR MP spectrum.

The IR MP absorption spectra (both measured and calculated) of the SF_6 molecules preliminarily excited into the QC are presented in Figure 5 for three values of the fluence Φ_2, namely, 0.5, 0.25, and 0.1 J/cm^2. The average level of preliminary excitation into the QC is taken to be $n_1 = 6$, which corresponds to a vibrational temperature of $T_{vib} = 960$ K reached by the instant the probe pulse arrives. The filled symbols in Figure 5a indicate the experimental N_2 values, and the solid and dashed curves represent the theoretical N_2 values calculated for γ_L defined by (13) and $\gamma_L = 0$, respectively. As noted earlier, consideration of the SIB effect alone provides for qualitative agreement between theory and experiment, there being quantitative differences increasing at the ends of the spectrum with increasing Φ_2. Taking at the same time account of the homogeneous broadening allows for quantitative agreement to be attained within experimental error.

The IR MP absorption spectra of Figure 5a were obtained with pump and probe pulses featuring a nonuniform intensity distribution in the transverse direction. The contribution from this nonuniformity is graphically illustrated by Figure 5b. The solid curve and filled symbols in this figure represent data for $\Phi_2 = 0.5$ J/cm^2 and $n_1 = 6$ for the Gaussian beams used. The dashed curve represents the calculation for a uniform transverse intensity distribution in both beams, made with the same Φ_2 and n_1 values. As can be seen, even the qualitative form of the IR MP spectrum changes—its maximum shifts quite substantially toward the "red" side. The reason for this deformation of the IR MP spectrum lies in the specifics of absorption at various frequencies ω_2. In the "red" wing of the IR MP spectrum, it is only the high-energy tail of the initial Boltzmann distribution that interacts with radiation (see below), and so, the distribution of n_1 being nonuniform, the main contribution to absorption comes from the central part of the probe beam, where fluence approximately corresponds to the average value of Φ_2. As a result, the difference between the homogeneous and inhomogeneous cases is relatively small. At the "blue" end, in interaction with radiation are the central and lower parts of the Boltzmann distribution, and so a material contribution to absorption (one-half and more for our probe beam profile[3]) is made by the central and lower parts of the Boltzmann distribution, where fluence is much lower than the average Φ_2 value. It is exactly this factor that makes the IR MP spectra at the "blue" end differ substantially between the homogeneous and inhomogeneous cases. Figure 5b demonstrates how important it is to take account of the actual spatial fluence distribution in the laser beams when comparing quantitatively between theoretical and experimental IR MP absorption spectra.

4. Discussion

As follows from the results presented, the prime objective of this work is attained. On the basis of comparison between experimentally measured and calculated spectra of IR MP absorption in the QC of the SF_6 molecule in the vicinity of the frequency of the mode ν_3, the relative contribution from the two types of broadening of the spectra, namely the SIB and homogeneous broadening, is revealed. It is demonstrated that consideration of only the SIB effect cannot help to fully describe IR MP spectra in the QC, especially at their ends. It is only simultaneous consideration of the homogeneous broadening that provides for a good agreement (within the accuracy of measurement) with experiment over a wide spectral and energy range. According with the initial assumption, the contribution from the SIB to the total width of the IR transition profile in fact materially exceeds the contribution from the homogeneous broadening, at least in the energy range 5000−15 000 cm^{-1}, where the determination of γ_L was most reliable (compare the solid curve with the top dashed curve in Figure 3).

But how reliable are the γ_L values obtained by us? As follows from the measurement and subsequent adjustment procedure described above, we tried to take account of all the factors that could affect the final result. From the principal standpoint, the reliability of determination of γ_L is governed by the reliability of the SIB parameters calculated. The spectral range selected by us is free from any strong resonances: the $\nu_2 + \nu_6$ and $\nu_5 + \nu_6$ bands are on the right and left of our range, respectively. Therefore, the use of the procedure developed in ref 1 for computing the transition profile parameters in the SIB approximation is quite appropriate. Next, the calculation of the inhomogeneous profile parameters is based on the use of the anharmonic constants x_{ij} whose values are determined, strictly speaking, for transitions near the ground state. The question arises as to the legitimacy of using these x_{ij} values for highly excited states. As follows from our measurements of the Raman spectra of the mode ν_1[2] and also the measurements taken in ref 13 of IR fluorescence spectra, these x_{ij} values "work" quite satisfactorily at vibrational temperatures $T_{vib} = 1700-2000$ K,

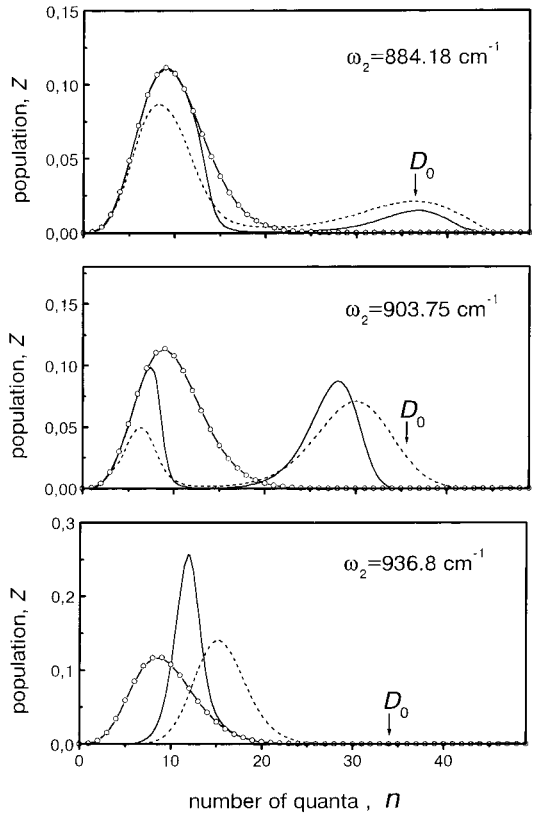

Figure 6. Vibrational distribution functions formed as a result of the IR MPE process for three values of the probe radiation frequency ω_2. Solid curves with circles: the initial Boltzmann distribution at $n_1 = 9$ quanta ($T_{vib} = 1242$ K). Solid curves: calculation with allowance made for the SIB effect only. Dashed curves: calculation with allowance made for both the SIB and homogeneous broadening effects. $\phi_2 = 0.25$ J/cm^2.

i.e., at mean energies $\langle E \rangle = 13\,500-17\,000$ cm^{-1}, as well. Proceeding from what has been said above, we believe that the γ_L values found in this work are reliable enough. It should be noted that the γ_L values obtained in the present work noticeably exceed the estimates of a "dissipative" part γ_d of the Lorentzian half-width made in ref 13 (compare the solid curve with the bottom dash-and-dot line in Figure 3), this "dissipative" part was attributed by the author of ref 13 to the intramolecular vibrational relaxation of the mode ν_3. At the same time, the obtained γ_L values are in rather good agreement with the estimates[13] of a complete half-width $\bar{\gamma}$ of the Lorentzian contour, including its "perturbative" part. However, the analysis of contribution of different interactions into the bandwidth of Lorentzian contour is the subject of special discussions and falls outside the scope of the present work.

The parameter measured experimentally in ref 3 is the energy absorbed in the course of IR MP excitation in the QC and *averaged over the entire molecular ensemble*. The same average parameter was in this work calculated theoretically and used to adjust theory and experiment. The characteristics of the profile of IR transitions in the QC found can be used to calculate the dynamics of IR MP excitation and find the "finer" characteristics of the process, specifically the function $Z = Z(n)$ of the vibrational distribution formed as a result of such an excitation. Figure 6 presents the vibrational distribution functions $Z(n)$ computed for the initial excitation level $n_1 = 9$ ($T_{vib} = 1242$ K), fluence $\phi_2 = 0.25$ J/cm^2, and a uniform spatial distribution of radiation. The functions $Z(n)$ are presented for three characteristic values of the frequency ω_2: approximately in the center ($\omega_2 = 903.75$ cm^{-1}), at the "red" end ($\omega_2 = 884.18$ cm^{-1}), and the "blue" end ($\omega_2 = 936.8$ cm^{-1}) of the IR MP spectrum (see Figure 5b). Presented in Figure 6 is the initial Boltzmann distribution (the curve with circles) and also the resultant distribution functions for a purely Gaussian transition profile (the solid curve), and the convolution of the Gaussian and a Lorentzian profiles (the dashed curve), parameters (13) of the latter being found in this work. Note that the *average* absorbed energy values for the given ϕ_2 and n_1 values at the frequencies $\omega_2 = 884.18$ and $\omega_2 = 936.8$ cm^{-1} are approximately the same. At the same time, as can be seen from Figure 6, the vibrational distribution functions for the frequencies selected differ even qualitatively. In the case $\omega_2 = 884.18$ cm^{-1} and $\omega_2 = 903.75$ cm^{-1}, the functions $Z(n)$ are of pronounced bimodal character, whereas for $\omega_2 = 936.8$ cm^{-1}, the function $Z(n)$ has a single maximum. Such a behavior of the function $Z(n)$ is due to the character of the relationship between the IR transition profile parameters and the molecular energy E (see Table 2). The analysis of this relationship shows that at the "blue" end of the IR MP spectrum, in interaction with radiation are the molecules from the lower and the central part of the Boltzmann distribution. As their excitation level grows higher, molecules fall off-resonance, so that their further excitation comes to an end. As the frequency of laser radiation is reduced, the molecules from the high-energy part of the initial distribution start interacting with it more and more effectively, and the level of their subsequent excitation grows higher. And at the very edge of the IR MP spectrum, it is only the far tail of the distribution that is interacting with radiation, but this small fraction of the molecules get excited highly. The same Figure 6 clearly demonstrates the effect of the Lorentzian wings associated with the homogeneous broadening, which is especially strong at the ends of the IR MP spectrum. It can be seen that these wings make for the "capture" of molecules from the lower states at the long-wavelength end, whereas at the short-wavelength end they provide for a higher excitation level of the molecules.

The bimodal character of the vibrational distribution formed as a result of IR MP excitation was observed directly or indirectly for various molecules in a number of experiments (for review, see refs 7 and 23) and is apparently a characteristic feature of multiple-step processes such as IR MPE. The reason for such a division of the distribution function is the presence of some "bottleneck" in the way of excitation of the molecules. There can be various particular mechanisms responsible for this "bottleneck". One of them is associated with the inhomogeneous character of interaction between radiation and the initial vibrational−rotational distribution. This may be a "rotational bottleneck" when some of the rotational levels interact with radiation stronger than others. A "vibrational bottleneck" is also possible, when some vibrational levels of the initial distribution interact with radiation stronger than other levels (for details, see ref 23). As can be seen from Figure 6, such a "vibrational bottleneck" may contribute noticeably to the formation of a double-hump bimodal distribution in the case of excitation of molecules in the quasicontinuum, especially at the "red" end of the IR MP spectrum ($\omega_2 = 884.18$ cm^{-1}). At the same time, our model computations show that there may be one more cause of formation of a double-hump distribution, namely, the initial state that may be a "bottleneck" itself. Indeed, if the rate at which molecules leave some initial state is lower than that of their subsequent excitation, starting with some level of the "ladder" of successive multiple-step transitions, then obviously there should occur a "discontinuity" in the distribution function. Such an effect occurs in the case of excitation at $\omega_2 = 884.18$

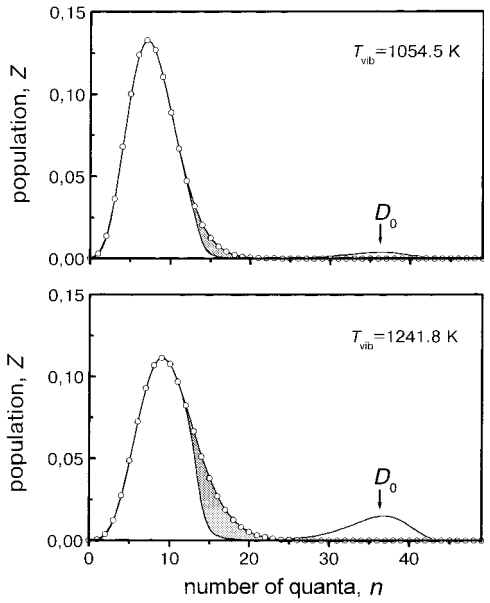

Figure 7. Vibrational distribution functions formed as a result of the IR MPE process for $T_{vib} = 1054$ K and $T_{vib} = 1242$ K. Solid curve with circles: the initial Boltzmann distribution. Solid curve: calculation in the SIB approximation for $\phi_2 = 0.25$ J/cm^2 and $\omega_2 = 884.18$ cm^{-1}.

cm^{-1} and $\omega_2 = 903.75$ cm^{-1} (Figure 6). Our calculations show that the double-hump form of the distribution function may remain even if the initial Boltzmann distribution in the QC is replaced with a monoenergetic one.

The knowledge of the cross sections of IR transitions in the QC enables one to optimize various processes induced by IR MP excitation, specifically the process of laser isotope separation. In the case of laser isotope separation based on IR MP dissociation, use is frequently made of a multicolor (multifrequency) excitation.[7,24,25] In that case, the energy consumption associated with the dissociation of the molecules is governed exactly by excitation in the quasicontinuum. That is why it is important to effect excitation in the quasicontinuum in an optimal fashion. Note in particular that if one properly chooses the frequency of radiation used to effect excitation in the quasicontinuum, one can even improve the initial selectivity of MP excitation from the ground state, which is provided by the first pulse. Indeed, if the vibrational temperatures (average energies) of two isotopic components differ after the passage of the first pulse, selecting the frequency ω_2 such that it is only the tail of the distribution prepared that interacts with radiation can noticeably improve the initial selectivity. These qualitative considerations support the results of calculation of the dynamics of IR MP excitation and dissociation of the SF_6 molecule within the framework of the model described. Figure 7 presents the resultant vibrational distribution of SF_6 molecules for two values of the initial vibrational temperature T_{vib}: 1054 K ($n_1 = 7$) and 1242 K ($n_1 = 9$). The calculation was made for $\phi_2 = 0.25$ J/cm^2 and $\omega_2 = 884.18$ cm^{-1} in the SIB approximation. It can clearly be seen that the fraction of excited molecules for the higher temperature is substantially greater (cf. the shadowed regions for $T_{vib} = 1242$ K and $T_{vib} = 1054$ K). The dissociation yields for these temperatures are $\beta_1 = 6.2\%$ and $\beta_2 = 1.57\%$, respectively, which gives a "selectivity" of $\alpha = \beta_1/\beta_2 = 3.95$. Allowing for the homogeneous broadening naturally reduces somewhat this selectivity improvement (as a result of the "capture" of molecules from lower vibrational states), but nevertheless the effect remains high enough: $\alpha = 2.85$ for the above conditions.

As follows from comparison between experimental data and results of calculation of IR MP excitation in the quasicontinuum, a qualitative agreement over a wide range of excitation conditions is observed only if the homogeneous broadening is taken into account. However, as already noted in the Introduction, the present-day theory cannot help calculate the homogeneous broadening parameters for a particular molecule. Nevertheless, as follows from the results of this work, one can, in principle, make correct quantitative calculations in that case as well, knowing only the SIB parameters. This conclusion directly follows from Figure 4. It can be seen that if account is only taken of the SIB effect, the error $\langle\Delta\rangle$ within some frequency range reaches its minimum and lies within the accuracy of measurement. This is due to the fact that the IR MP excitation process at these frequencies and within the fluence range selected proceeds so that the radiation frequency does not fall, as the molecule moves up the "ladder" of vibrational states, outside the central part of the Gaussian transition profile, and so the role of the wings, where the effect of the homogeneous broadening may be decisive, is still insignificant. Therefore, when describing multicolor IR MP excitation in the quasicontinuum, one can restrict oneself to the use of the SIB approximation and calculate the transition cross section parameters by the procedure suggested in ref 1, provided that each radiation pulse at the corresponding frequency "works" largely within the limits of the central part of the transition profile.

5. Conclusion

Comparison is made between experimentally measured and theoretically calculated IR MP excitation spectra in the quasicontinuum of the SF_6 molecule in the vicinity of the frequency of the mode ν_3. The calculation is carried out within the framework of the model developed, based on the rate equations approximation and allowing for the rotational structure of IR transitions. The cross sections of the successive transitions are computed in the statistical inhomogeneous broadening approximation on the basis of a procedure developed earlier. A good agreement (within the accuracy of measurement) is achieved between the experimentally measured and calculated IR MP absorption spectra over wide spectral and energy ranges. The special importance was revealed of the allowance for the spatial distribution of radiation in making such a quantitative comparison.

As a result of the comparison made between theory and experiment, the main objective of this work is attained, namely, the relative contribution is revealed from the SIB and homogeneous broadening effects to the shape of the transition profile in the QC near the frequency of the ν_3 mode of SF_6. The values of the half-width γ_L are found in the energy range $4500 \leq E \leq 30\,000$ cm^{-1}. It is shown that the main contribution to such IR transition profile parameters as the position of its maximum, width, and intensity comes from the SIB effect, but the Lorentzian wings may play a decisive role when the excitation of the molecules takes place at an edge of the spectrum.

The IR transition cross sections obtained in this work are used to compute the dynamics of IR MPE in the quasicontinuum and determine the vibrational distribution function formed as a result of this process. It is found that excitation in the QC may give rise to a nonequilibrium bimodal distribution. The conclusion is drawn that the selectivity attained at the first stage of multicolor LIS can be improved by appropriately selecting the excitation frequency.

By and large, the results of this work show that at present one can make a quantitative model description of the dynamics

TABLE 3: Fundamental Vibrational Frequencies of the Activated Complex $SF_6^\dagger$ and Their Assignment

		Data of ref 26		Present work	
SF_6 symmetry	$SF_6^\dagger$ symmetry	$i^\dagger$	$\nu^\dagger_i$, cm^{-1}	$i^\dagger$	$\nu^\dagger_i$, cm^{-1}
A_{1g}	A_1	2	735.30	2	580.5
E_g	A_1	3	481.50	4	*a*
	B_1	5	609.90	5	609.90
F_{1u}	A_1	1	711.00	1	711.00
	E	8	900.60	8	900.60
F_{1u}	A_1	4	*a*	3	584.25
	E	9	584.25	9	584.25
F_{2g}	B_2	7	496.85	7	496.85
	E	10	392.25	10	392.35
F_{2u}	B_1	6	259.50	6	259.50
	E	11	328.70	11	259.50

[a] Reaction coordinate.

of IR MP excitation in the quasicontinuum of molecules and restrict oneself in a number of cases to the use of the SIB approximation for the purpose.

Appendix A

The unimolecular decay rate constants $k(E)$ in (8) and (9) were computed within the framework of the RRKM theory. The work reported in ref 26 presents the frequencies of the activated complex $SF_6^\dagger$, as well as the $k(E)$ values. However, we found a discrepancy between the frequencies of the complex presented by the author of ref 26 in Table 2 and the final results of calculation of $k(E)$ in Figure 3. Moreover, we found that the frequency values in Table 2 contradicted the physical substantiation of their determination given in the text of ref 26. Nevertheless, we believed that the above argument was quite justified and used it to construct another model of the activated complex. This model was found to yield $k(E)$ values close to those presented in ref 26. The frequencies of the activated complex obtained in the given work and presented in ref 26 are listed in Table 3.

Appendix B

For numerical integration of equations (8), we utilized the time propagation technique using the polynomial approximation of the evolution operator,[27] which is especially powerful for the large sparse sets of equations. Representing populations N_{nJ} in a vector form as $|z\rangle$ and rewriting (8) and its solution in a conventional matrix form, we have

$$\mathrm{i}\frac{\mathrm{d}|z\rangle}{\mathrm{d}t} = \hat{H}|z\rangle \qquad |z(t)\rangle = (-\mathrm{i}\hat{H}t)|z(0)\rangle \tag{B1}$$

where the matrix $\hat{W}$ of our set of equations is $\hat{W} = -\mathrm{i}\hat{H}$, by definition. For the Hamiltonian systems with real eigenvalues of $\hat{H}$, good convergence is guaranteed by the following expansion of the evolution operator in the Chebyshev polynomials:

$$\exp(-\mathrm{i}\hat{H}t) \approx \exp\left[-\frac{\mathrm{i}}{2}(\epsilon_{\max}+\epsilon_{\min})t\right]\sum_{n=0}^{N}\mathrm{i}^n(2-\delta_{n0})J_n \times \left[\frac{1}{2}(\epsilon_{\max}+\epsilon_{\min})t\right]T_n\left(\frac{2\hat{H}-\epsilon_{\max}-\epsilon_{\min}}{\epsilon_{\max}-\epsilon_{\min}}\right) \tag{B2}$$

Here $\epsilon_{\min}$ and $\epsilon_{\max}$ are respectively the minimum and maximum $\hat{H}$ eigenvalues; J_n are Bessel functions; the operator in the braces at T_n is normalized so that its eigenvalues are positioned from -1 to $+1$. Exact equality in (B2) formally takes place at $N \to \infty$.

In our case, however, the $\hat{W}$ *eigenvalues are real and nonpositive*, so the $\hat{H}$ eigenvalues are positioned on the negative imaginary semiaxis. Then, as told in ref 28, exploration of the approximation like (B2) does not provide adequate convergence, and other polynomial approximations are recommended. Nevertheless, our investigation showed that convergence can be significantly improved by shifting the eigenvalues into the positive imaginary semiaxis.

In general,[27] accuracy of the Chebyshev polynomial approximation may be estimated through that of the expansion of the relevant scalar function

$$\exp(-\mathrm{i}x\tau) = \sum_n \mathrm{i}^n(2-\delta_{n0})J_n(\tau)T_n(x) \tag{B3}$$

with the dimensionless parameters $\tau \gg 1$ and $|x| \sim 1$. The value of τ defines, in fact, the necessary number $(N+1)$ of the terms in (B3) that can be optimized using the known asymptotic properties of the Bessel functions. We varied the purely imaginary parameter x, choosing two tolerance values $\theta^{(1)} = 10^{-5}$ and $\theta^{(2)} = 10^{-10}$, to compare the result of computation in the right side of (B3) with the exact value in the left side of (B3). Values of x that comply with any of these tolerance criteria lie inside some interval in the imaginary axis including $x = 0$, and the maximally allowed negative value $|x|^{(-)}_{\max}$ proves to be essentially less than the maximally allowed positive value $|x|^{(+)}_{\max}$. The calculated dependences $|x|_{\max}(\tau)$ are shown in Figure 8. In addition, dependence of the value $|x|_{\max}\tau/N$ on τ, which characterize the method efficiency, is presented in this figure.

Let us return explicitly to our original notation

$$\frac{\mathrm{d}|z\rangle}{\mathrm{d}t} = \hat{W}|z\rangle \tag{B4}$$

A conclusion can be drawn from the obtained results that, for better efficiency of the method, one should transform the matrix $\hat{W}$ to bring its eigenvalues from the negative imaginary semiaxis to the positive one. This is achieved by the substitution $\hat{W} = \hat{\tilde{W}} + \lambda_0\hat{I}$ where $\hat{I}$ is the unity matrix, and λ_0 is the minimum eigenvalue of $\hat{W}$. The latter can be found rather easily with the well-known Lanczos algorithm. Next, wishing to reach the calculation tolerance of, e.g., $\theta^{(2)} = 10^{-10}$, one can see from Figure 8c that it is rather optimum to divide $\hat{\tilde{W}}$ by $2|\lambda_0|$. Then, for direct application of the integration formula $|z(t+\Delta t)\rangle = \exp(\hat{W}\Delta t)|z(t)\rangle$, the time step Δt should not exceed the value $\Delta t_{\max} \approx 100/\lambda_0$. Finally, the formula of the computational algorithm is

$$|z(t+\Delta t\rangle = \exp(|\lambda_0|t)[\sum_{n=0}^{N}\mathrm{i}^n(2-\delta_{n0})J_n(2|\lambda_0|\Delta t)\hat{T}_n]|z(t)\rangle \tag{B5}$$

where the matrices $\hat{T}_n$ are

$$\hat{T}_n = T_n(\hat{W}_{\mathrm{norm}}) \qquad \left(\hat{W}_{\mathrm{norm}} = \mathrm{i}\frac{\hat{W}+|\lambda_0|\hat{I}}{2|\lambda_0|}\right) \tag{B6}$$

Realization of the algorithm is standard. Transformations (B5), which are equivalent to the time propagation of (B4), are performed with the step of $\Delta t \le \Delta t_{\max}$ starting from the vector $|z(0)\rangle$ (initial population distribution). Products of the matrices (B.6) on the vector $|z(t)\rangle$ are successively found using the

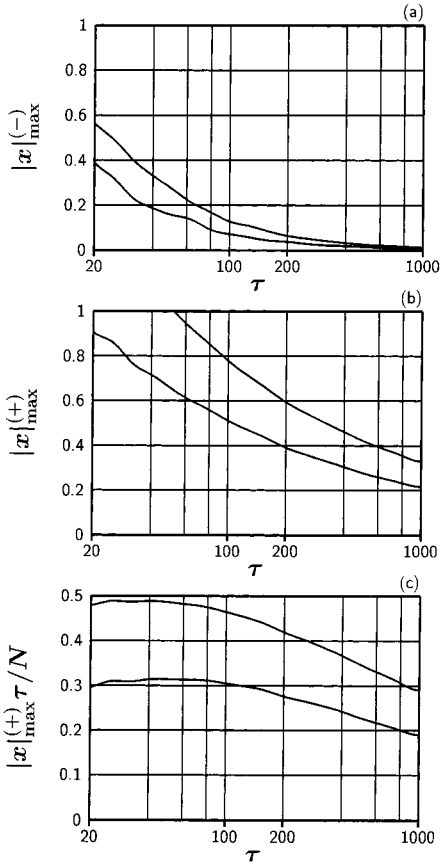

Figure 8. Characteristics for the approximation (B.3) of the function $\exp(-ix\tau)$ with the real parameter τ, and x placed on the imaginary axis. For all graphs, the upper curves are for the relative accuracy of $\theta^{(1)} = 10^{-5}$, and lower curves are for the relative accuracy of $\theta^{(2)} = 10^{-10}$. (a) Maximally allowed negative imaginary value of x depending on τ. (b) Maximally allowed positive imaginary value of x depending on τ. (c) The value $|x|^{(+)}_{max}\tau/N$ as the function of τ for $ix < 0$.

recurrence formula $\hat{T}_{n+1}|z(t)\rangle = 2\hat{W}_{norm}\hat{T}_n|z(t)\rangle - \hat{T}_{n-1}|z(t)\rangle$ and, after multiplication on the corresponding coefficient, are accumulated in the array $|z(t + \Delta t)\rangle$. The recurrence formula is turned on after the calculation of $\hat{T}_0|z\rangle = |z\rangle$ and $\hat{T}_1|z\rangle = \hat{W}_{norm}|z\rangle$.

References and Notes

(1) Makarov, A. A.; Petrova, I. Yu.; Ryabov, E. A.; Letokhov, V. S. *J. Phys. Chem. A* **1998**, *102*, 1438.
(2) Malinovsky, A. L.; Petrova, I. Yu.; Ryabov, E. A.; Makarov, A. A.; Letokhov, V. S. *J. Phys. Chem. A* **1998**, *102*, 9353.
(3) Lokhman, V. N.; Petin, A. N.; Ryabov, E. A.; Letokhov, V. S. *J. Phys. Chem. A* **1999**, *103*, 11293.
(4) Grant, E. R.; Coggiola, M. J.; Lee, T. Y.; Schultz, P. A.; Sudbo, Aa. S.; Shen, Y. R. *Chem. Phys. Lett.* **1977**, *52*, 595.
(5) Quack, M. *J. Chem. Phys.* **1978**, *69*, 1282.
(6) Quack, M. *Adv. Chem. Phys.* **1982**, *50*, 395.
(7) Bagratashvili, V. N.; Letokhov, V. S.; Makarov, A. A.; Ryabov, E. A. *Multiple Photon Infrared Photophysics and Photochemistry;* Harwood Academic Publishers: Chur, Switzerland, 1985.
(8) Goodman, M. F.; Stone, J.; Thiele, E. In *Multiple-Photon Excitation and Dissociation of Polyatomic Molecules;* Cantrell, C. D., Ed.; Topics in Current Physics, Vol. 35; Springer: Berlin, 1986; p 159.
(9) Quack, M. *Infrared Phys.* **1989**, *29*, 441.
(10) Bagratashvili, V. N.; Doljikov, V. S.; Letokhov, V. S.; Makarov, A. A.; Ryabov, E. A.; Tyacht, V. V. *Sov. Phys.-JETP* **1979**, *50*, 1075.
(11) Horsley, J. A.; Stone, J.; Goodman, M. F.; Dows, D. A. *Chem. Phys. Lett.* **1979**, *66*, 461.
(12) Makarov, A. A.; Makarov, G. N.; Puretzky, A. A.; Tyakht, V. V. *Appl. Phys.* **1980**, *23*, 1980.
(13) Angelié, C. *J. Chem. Phys.* **1993**, *98*, 2541.
(14) McDowell, R. S.; Krohn, B. J.; Flicker, H.; Vasquez, M. C. *Spectrochim. Acta* **1986**, *42A*, 351.
(15) Alimpiev, S. S.; Sartakov, B. G. *Laser Chem.* **1992**, *12*, 147.
(16) McDowell, R. S.; Krohn, B. J. *Spectrochim. Acta* **1986**, *42A*, 371.
(17) Fox, K.; Person, W. B. *J. Chem. Phys.* **1976**, *64*, 5218.
(18) Makarov, A. A. In *Laser Spectroscopy of Highly Vibrationally Excited Molecules*; Letokhov, V. S., Ed.; Adam Hilger: Bristol, New York, 1989; p 106.
(19) Bobin, B.; Bordé, C. J.; Bordé, J.; Bréant, C. *J. Mol. Spectrosc.* **1987**, *121*, 91.
(20) Akhmanov, S. A.; Gordienko, V. M.; Lazarev, V. V.; Micheenko, A. V.; Panchenko, V. Ya. *Sov. Phys.-JETP* **1980**, *51*, 1087.
(21) Becker, F. S.; Kompa, K. L. *Nucl. Technol.* **1982**, *58*, 329.
(22) Dolzhikov, Yu. S.; Letokhov, V. S.; Makarov, A. A.; Malinovsky, A. L.; Ryabov, E. A. *Sov. Phys.-JETP* **1986**, *63*, 1161.
(23) Ryabov, E. A. In *Laser Spectroscopy of Highly Vibrationally Excited Molecules*; Letokhov, V. S., Ed.; Adam Hilger: Bristol, New York, 1989; p 55.
(24) Lyman, J. L. In *Laser Spectroscopy and its Applications*; Radziemski, J. L., Solarz, R. W., Raisner, J. A., Eds.; Dekker: New York, 1987; p 417.
(25) Evseev, A. V.; Letokhov, V. S.; Puretzky, A. A. *Appl. Phys.* **1985**, *B39*, 93.
(26) Lyman, J. L. *J. Chem. Phys.* **1977**, *67*, 1868.
(27) Kosloff, R. *Annu. Rev. Phys. Chem.* **1994**, *45*, 145.
(28) Ashkenazi, G.; Kosloff, R.; Ruhman, S.; Tal-Ezer, H. *J. Chem. Phys.* **1995**, *103*, 10005.